IEEE Access
Multidisciplinary | Rapid Review | Open Access Journal

SPECIAL SECTION ON SMART HEALTH SENSING AND COMPUTATIONAL INTELLIGENCE: FROM BIG DATA TO BIG IMPACTS

Received March 15, 2019, accepted May 14, 2019, date of publication May 22, 2019, date of current version June 5, 2019.

*Digital Object Identifier 10.1109/ACCESS.2019.2918292*

# Unsupervised Detection of Apnea Using Commodity RFID Tags With a Recurrent Variational Autoencoder

**CHAO YANG[1], XUYU WANG[2], AND SHIWEN MAO[1], (Fellow, IEEE)**
[1]Department of Electrical and Computer Engineering, Auburn University, Auburn, AL 36849-5201, USA
[2]Department of Computer Science, California State University, Sacramento, CA 95819-6021, USA

Corresponding author: Shiwen Mao (smao@ieee.org)

This work was supported in part by the U.S. NSF under Grant CNS-1702957, and in part by the Wireless Engineering Research and Education Center (WEREC), Auburn University, Auburn, AL, USA.

**ABSTRACT** With the rapid development of intelligent health sensing in the Internet of Things (IoT), vital sign monitoring (e.g., respiration) and abnormal respiration detection have attracted increasing attention. Considering the challenging and the cost of collecting labeled training data from patients with breathing related diseases, we develop the AutoTag system, an unsupervised recurrent variational autoencoder-based method for respiration rate estimation and abnormal breathing detection with off-the-shelf RFID tags. Moreover, for real-time breath monitoring, a novel method is proposed to cancel the distortion on measured phase values caused by channel hopping for FCC-complaint RFID systems. The efficacy of the proposed system is demonstrated by the extensive experiments conducted in two indoor environments, while the impact of various design and environmental factors is also evaluated.

**INDEX TERMS** Apnea, deep learning, radio-frequency identification (RFID), recurrent variational autoencoder, respiration monitoring.

## I. INTRODUCTION

The population is aging in many parts of the worlds. Consequently, smart healthcare has attracted increasing concerns [1]–[4]. Rather than going to hospital after getting sick, people are intend to early detect and prevent diseases by monitoring their vital sings on daily basis. For example, One of the breathing disorders is obstructive sleep apnea, which can imply serious health problems in human body including high blood pressure, heart disease, and sudden infant death syndrome (SIDS) for sleeping infants [5]. However, in traditional healthcare systems, vital signs are measured by dedicated equipment like capnography [6], which is not convenient for all-day monitoring, especially when the patient is sleeping. Moreover, the breathing abnormality diagnosis may consume considerable efforts and experience from medical institution. Therefore, autonomous, low-cost, unobtrusive vital sign monitoring methods that can detect abnormality are desired for IoT based smart healthcare systems, which can benefit many people for monitoring health conditions in their daily life.

Considering the mobility and flexibility of RF devices, wireless signals are widely used on smart healthcare systems to monitor human vital signs. Since the movement of human chest and heart can slightly affect the propagation of RF signals, the signal of breathing and heartbeat can be reconstructed by analyzing the change in received RF signals. Based on this basic idea, multiple existing techniques incorporate a radar for respiration monitoring, including frequency modulated continuous wave (FMCW) radar [7] and Doppler radar [8], but at a relatively high cost due to the special hardware. To achieve low cost RF system, WiFi based techniques are developed for heath sensing with commodity WiFi devices. Rather than directly analyzing received signals from radar, WiFi based techniques leverage either Received Signal Strength (RSS) [9] or Channel State Information (CSI) [10]–[13] collected from the device driver. Although the WiFi techniques are low-cost and flexible, the systems are sensitive to the noise caused by surrounding environment, such as moving objects or persons nearby. The accuracy of such systems is relatively low in unstable environments.

The associate editor coordinating the review of this manuscript and approving it for publication was Qingxue Zhang.

The low-cost and near-field features of passive RFID tags have triggered great interest on apply them for health sensing. Some RFID based systems are proposed to achieve low cost as well as reducing the influence of unstable surroundings. Multiple RFID based techniques have been developed for object tracking [14], orientation estimation [15], drones [16]–[18], and especially, for respiration monitoring [19]. Such existing works mainly make use of the RFID phase information collected from the RFID reader on different channels. One such typical techniques for smart healthcare is called TagBreathe, which monitors the respiration signal of a patient by grouping the RFID responses collected from the same channel and using a estimated displacement in each channel [19]. This method may not be well suited for operation with Ultra High Frequency (UHF) RFID devices in the US, which all adopt frequency hopping over 50 channels, 200 ms per channel, according to FCC requirements. When the reader and tag hop among 50 channels, it will take 10 seconds for them to return to the same channel. To collect a sufficient amount of readings from the same channel, the delay will be considerable, making it hard for real-time detection of abnormality (e.g., apnea).

To address this issue, we present the AutoTag system, an unsupervised recurrent variational autoencoder method for respiration rate estimation and abnormal breathing detection with off-the-shelf RFID Tags. To mitigate the effect caused by channel hopping, we propose a novel technique to map the RFID phase values collected from multiple different channels to a single reference channel. Since FCC requires the RFID system to hop to a different channel every 200 ms, a typical RFID based sensing system can hardly be applied for real-time monitoring of patients' vital signs. Rather than offline calibration employed in Tagyro [14], our method can enable real-time phase calibration, which is amenable to dynamic environments. Furthermore, compared with the method used in TagBreathe, our method incurs much lower delay, because grouping data for all channels is not needed with our technique.

Furthermore, we develop an unsupervised deep learning approach for apnea detection, which can autonomously detect abnormality in human respiration. Recently, a recurrent variational autoencoder model has been successfully applied to sequence modeling [20] and human motion synthesis [21]. Inspired by these works, we develop an enhanced recurrent variational autoencoder model for detection of breathing abnormality, such as apnea. With the proposed approach, abnormality can be detected by evaluating how similar the sampled breathing signal and reconstructed signal using the deep learning network are. Our method is superior to the traditional energy-threshold based approach, since the testing environment may not be absolutely stationary. Our proposed method can easily distinguish non-periodic signals from normal periodic signal by learning the features of normal breathing signals, while the energy based method only consider apnea as a relative weak signal compared with normal cases. Since the proposed scheme is an unsupervised learning, it has the desirable advantage of not requiring labeled medical data, which is usually costly and time-consuming to obtain.

Specifically, we present the AutoTag system, a recurrent variational **Auto**encoder for respiration rate estimation and unsupervised detection of apnea with commercial passive UHF RFID **Tag**s. The AutoTag system composes of three main components, including (i) the signal extraction module, (ii) the calibration module, and (iii) the breathing monitoring module. The phase data is firstly collected from a commodity RFID reader by the signal extraction module. The calibration module is mainly used for calibration of the sampled breathing data, while the respiration monitoring module is designed for estimating the patient's respiration rate and detecting abnormalities such as apnea. We prototype the AutoTag system using a platform of commercial RFID tags and reader, and conduct extensive experiments in two different environments with four volunteers. We observe superior performance achieved by the proposed AutoTag system in these experiments. The impact of various design and environment factors are also tested in corresponding experiments.

We summarize the three main contributions of this work as follows.

- To our best knowledge, the AuTotag system is the first apnea detection systems incorporating an enhanced recurrent variational autoencoder model. The proposed scheme is an unsupervised learning, with the desirable advantage of not requiring costly labeled medical data.
- We also propose a novel technique to address the frequency hopping offset, which is a real-time calibration. The proposed scheme is simple but effective in mitigating the frequency hoping offset, thus enabling many real-time sensing applications for FCC-compliant RFID readers and tags.
- We design and prototype the AutoTag system, which is composed with (i) signal extraction, (ii) data calibration, and (iii) respiration monitoring modules, and evaluate the system in two different representative healthcare environments. We present our experimental results that validate the efficacy of the proposed AutoTag system.

The mainder of this paper is organized as follows. The related work is reviewed in Section II, and preliminaries of RFID based sensing is discussed in Section III. The AutoTag system design is presented in detail and analyzed in Section IV. The experimental performance evaluation of the proposed system is provided in Section V. We conclude this paper in Section VI.

## II. RELATED RESEARCH

The AutoTag system is mostly related to RF signal based vital sign monitoring systems and RFID based sensing. We briefly introduce these two classes of related work in this section.

Nowadays, many RF based systems have been proposed to monitor vital signals of human, which are developed on different types of platforms, including Radar systems, WiFi systems, and RFID based systems. The Radar technique is a straightforward way to identify the fluctuation of human chest

caused by respiration, because Radar can directly monitor the distance variation between the human chest and the device antenna. One of the representative works in this category leverages an FMCW radar to monitor respiration rate and heart rate for multiple users simultaneously [7]. Furthermore, other Radar based systems have also been proposed to measure human respiration, including Doppler radar [8] and ultra wideband (UWB) Radar [22]. These radar based systems can accurately detect vital signs, and the influence caused by surroundings is limited. However, since the special hardware is essential to such systems, the cost of such systems are usually high, hampering their wide deployment such as in homes.

To achieve low cost and ease of deployment for vital sign monitoring, WiFi based techniques have been utilized to measure both human breathing rate and heart rate. The human respiration and heartbeat can be extracted by analyzing variations in WiFi channels, for example, the RSS as in Ubibreathe [9]. However, the Ubibreathe system requires the patient to stand between the transmitter and the receiver, while some other CSI based techniques have no such strict requirements. Different from RSS based systems, CSI can provide fine-grained channel inforamtion, and can achieve higher resolution and sensitivity than RSS for monitoring human vital signs. One of the CSI based techniques can leverage amplitude of CSI to monitor breathing rate and heart rate when the patient is sleeping [10]. In addition to the amplitude, the CSI phase information can also carry human respiration signal [11]. Furthermore, the TensorBeat system can estimate respiration rates for multiple persons crowed in a small space [12], by incorporating tensor decomposition on the collected CSI phase data. Although WiFi based techniques can measure human vital signs with off-the-shelf WiFi devices, the accuracy is easily affected by the surrounding environment, because of broadcasting nature and long range of WiFi transmissions. To address this issue, some RFID based systems like TagBreathe are developed to track human respiration by analyzing the RFID response data collected at an RFID reader [19]. Since the passive UHF RFID tags are low-cost and are easily attachable to human body, the RFID system can monitor human vital signs at a low cost and is resilient to interference from the unstable environment.

Apart from RFID based vital sign monitoring systems, various sensing systems are proposed by leveraging the data extracted from the low level protocol in RFID systems, such as RSS and phase values, which have been utilized for many applications, e.g., indoor localization. For RSS based methods, one of the representative techniques estimates the tag position by comparing the RSS from the target tag with reference tags [23]. Moreover, another technique can obtain the refined tag position by utilizing the characteristics of the coupling effect on RSS [24]. However, due to the low resolution of RSS, developing an RSS based localization scheme with high accuracy is challenging. Thus, many phase based localization techniques are proposed. One of the typical phase based methods has been developed for estimating distance with direction of arrival (DOA) [25], but the result has a relatively large ambiguity because of the periodicity of measured phase. To remove the ambiguity, some other techniques are proposed to obtain the more accurate position than the typical method by leveraging the aperture radar technique [26] and hologram technique [14], [27], [28]. Besides indoor localization, RFID tags are also widely used for other sensing techniques such as remote control of drones [16]–[18], object orientation estimation [15], remote temperature measurement [29], and gesture recognition [30].

## III. PRELIMINARIES OF RFID SNSING

According to FCC regulations, UHF RFID readers should use channel hopping to avoid co-channel interference. The spectrum from 902.5 MHz to 927.5 MHz is partitioned into 50 non-overlapping channels, and the reader remains on each channel for 200 ms. Usually such frequency hopping introduces an additional phase offset in the RFID response signal, causing large errors in RFID based sensing.

According to the manual of RFID reader, e.g., [31], the phase $\phi$ of the received RFID response signal can be expressed as

$$\phi(f_i, d) = \mathrm{mod}\left(\frac{2\pi f_i d}{c} + \delta_T + \delta_R + \delta_{Tag}, 2\pi\right), \quad (1)$$

where $d$ is the total distance from the reader's antenna to the tag and then back to the reader antenna, $f_i$ is the frequency of channel $i$, $c$ is a constant representing the speed of light, and $\delta_T$, $\delta_R$, and $\delta_{Tag}$ are the phase offsets caused by the transmitter circuit, the receiver circuit, and the tag's reflection characteristics, respectively.

For Impinj R420, a commodity RFID reader, the phase offset between two adjacent channels that it hops to is not a constant, even though the distance $d$ rmains the same, as found in our experimental studies. Since the three offsets in (1) are irrelevant to the distance $d$, we can lump the three offsets into a single variable $\delta_i$ for each channel $i$. The phase $\phi(f_i, d)$ for channel $f_i$ under round-trip distance $d$ can thus be expressed as

$$\phi(f_i, d) = \mathrm{mod}\left(\frac{2\pi f_i d}{c} + \delta_i, 2\pi\right). \quad (2)$$

The main challenge for extracting the breathing signal from the RFID phase measurements is how to mitigate the discontinuity in phase data, which is caused by channel hopping. One way to eliminate the channel hopping influence, as proposed for the TagBreathe system [19], is to group the signals collected from the same channel and to use the estimated displacement in each channel to track the breathing signal. As discussed earlier, this method may not work well for RFID systems in the US, since the reader must hop among 50 different frequencies, following the FCC requirement. Fig. 1 plots the change of channel index in a period of 30 seconds. We can see that it takes about 10 seconds for the antenna to hop through all the 50 channels. Thus, the TagBreathe method will take a very long time to collect and group multiple phase

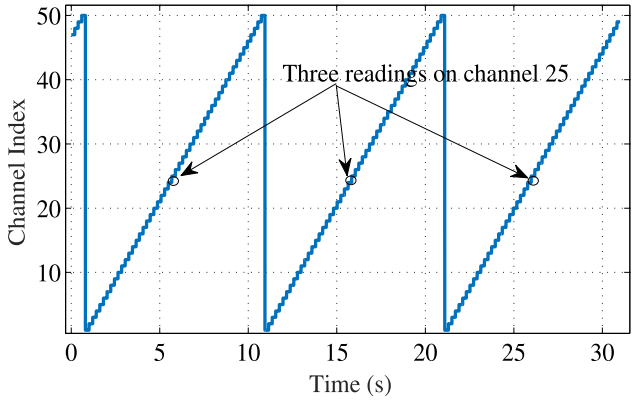


**FIGURE 1.** The channel indexes used by an FCC-compliant RFID reader during a period of 30 seconds.

readings on the same channel, leading to extremely long delay in respiration measurement with FCC-compliant readers.

To address the extremely long delay caused by channel hopping among 50 different frequencies, the Tagyro system calibrates phase values collected from all channels based on one reference channel [15]. Specifically, the Tagyro technique first measures the phase offset $\delta_i$ for all the 50 channels. Then, the phase offset introduced by channel hopping can be removed by subtracting the phase offset $\delta_i$ in each channel. This method is suitable for a static environment; but it may not be effective for tracking human breathing signal and apnea, where the tags are mounted on the human body and moves as the patient breaths. This is because the wireless channel will change if the patient moves (even slightly). The movement causes an additional offset in $\delta_i$, so that the estimated phase offset $\hat{\delta}_i$ does not match the real-time $\delta_i$ after the small movement.

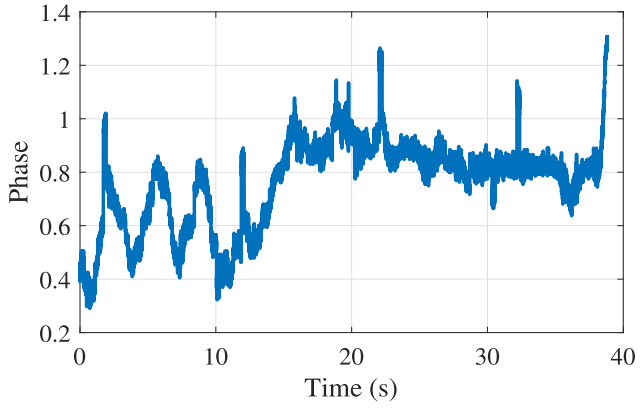


**FIGURE 2.** Calibrated phase obtained using the Tagyro method [15].

Fig. 2 plots the calibrated phase data obtained with the Tagyro method. It can be observed that the breathing signal can be detected in the beginning (i.e., the first 15 seconds), because the initial phase offset is correct. After the first 15 seconds, the breathing signal cannot be detected, because the channel hopping effect cannot be perfectly mitigated. To continuously eliminate the frequency hopping effect, we propose a new method in the proposed AutoTag system, to update and remove the phase offset $\delta_i$ in real-time for breathing and apnea detection.

## IV. DESIGN AND ANALYSIS OF THE AUTOTAG SYSTEM

### A. DESIGN OF THE AUTOTAG SYSTEM

The AutoTag system aims to measure human respiration and detect breathing abnormalities, such as apnea, with multiple RFID tags attached to the patient's body (i.e., clothes). As given in (1), the collected phase information is indicative of the round-trip distance $d$ between the reader antenna and the corresponding tag. When the patient breaths, the distance $d$ changes slightly with the chest movements. Thus, by analyzing the phase variations collected from the tags attached to the human body, we can obtain the periodic signals caused by chest movements. However, for accurately measuring the human respiration rate and precisely detecting apnea, several challenges should be addressed, such as mitigating the channel hopping effect, the sensitivity divergence for different tags, and dealing with the interference from surroundings. To address these issues, we incorporate three modules in the AutoTag system, including (i) signal extraction, (ii) data calibration, and (iii) respiration monitoring, as illustrated in Fig. 3.

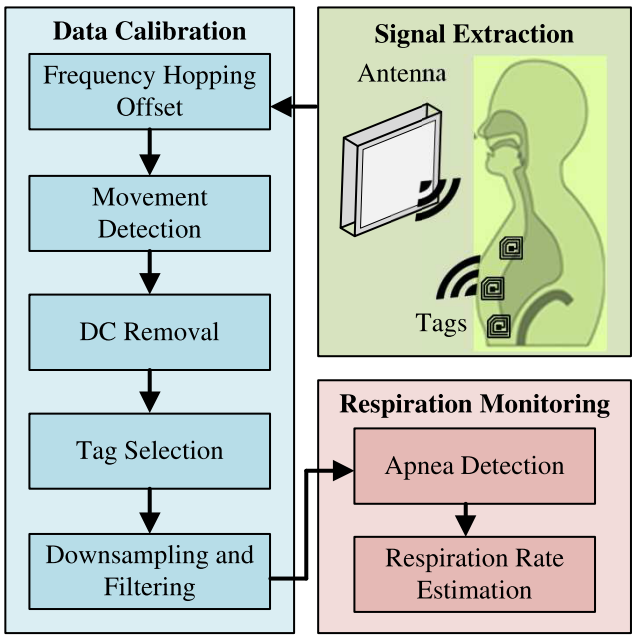


**FIGURE 3.** The AutoTag system architecture, which includes signal extraction, data calibration, and respiration monitoring.

In the signal extraction module, we extract the phase data from the received responses from three tags attached to the human body, using a directional antenna at the reader. In the following *data calibration* module, we firstly remove the influence caused by channel hopping of the RFID reader. Then we detect whether the monitored patient is moving

or not based on a threshold based method, i.e., movement detection. After that, we remove the DC component from the selected signal to eliminate the impact of small movements of the patient. Then, tag selection is implemented to choose the tag with the strongest signal strength. Finally, we apply down-sampling and filtering to obtain the final respiration signal. In the respiration monitoring module, we adopt a recurrent variational autoencoder for detection of abnormalities such as apnea. Our approach is an unsupervised learning, which has the great advantage of not requiring labeled medical data, which is extremely costly to collect. The respiration rate can also be estimated with a peak detection method when the patient is breathing normally. We will introduce the detailed design of each module in the remainder of this section.

### B. SIGNAL EXTRACTION

As shown in Fig. 3, the first module is used for extracting low-level phase readings from received tag responses. The movements of the patient's chest and abdomen induced by breathing, cause the tag-reader antenna distance to vary with human respiration. The time-varying distance translates to the time-varying phase in the tag response signal, which is indicative of the respiration signal. To increase the system's robustness, three passive UHF RFID tags are attached to the upper body of the patient. The RFID reader uses a directional antenna to transmit RF interrogating signals to the tags and to read low-level data from the backscattered signals from the tags, which includes time stamp, phase, received signal strength indicator (RSSI), and Doppler shift.

For most RFID systems, the collected RSSI data usually has a very low resolution, and the signal-to-noise ratio (SNR) of Doppler shift is usually low. Thus these two types of information are not very helpful for detecting the respiration signal. In AutoTag, we focus on the collected phase information from RFID responses for respiration rate estimation and apnea detection.

### C. DATA CALIBRATION

The captured phase information cannot be directly used for detecting the respiration signal. In Fig. 4, we plot the uncalibrated phase data received from one of the reader antennas for a duration of 28 s. It can be observed that when the reader hops around various channels (200 ms on each channel), the measured phase data exhibits a wide range of variations. Furthermore, there is a large offset incurred in the phase data when the frequency hopping happens. It is thus highly challenging to extract the weak respiration signal from such uncalibrated data. The raw phase data should be calibrated first to facility the extraction of the respiration signal.

#### 1) MITIGATING THE FREQUENCY HOPPING OFFSET

We unwrap the captured phase signal to remove the offset introduced by the modulo operation in (2). With the modulo operation, a slight change in the real phase may lead to a large jump in the received phase signal. For instance, a small change of the real phase from $0.1\pi$ to $-0.1\pi$ will cause

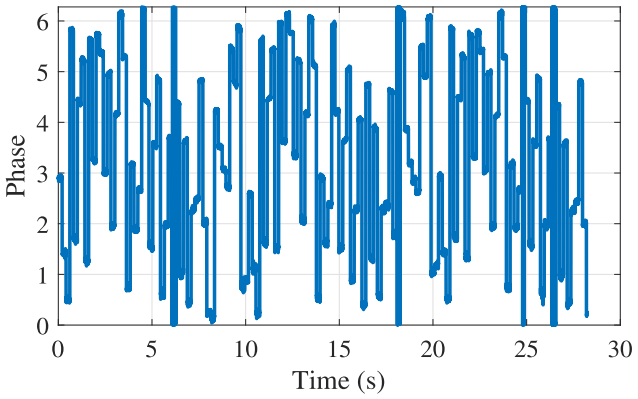


**FIGURE 4.** Uncalibrated phase data collected from a tag for a duration of 28 s.

the received phase to change from $0.1\pi$ to $1.9\pi$. Since the sampling rate of the reader is usually higher than 100 Hz for each tag in our system, the interarrival time of phase samples is usually smaller than 0.01 s. Assuming that the phase value change of two back-to-back readings is smaller than $\pi$ under such a small interarrival time, $\pm 2\pi$ can be added to recover the original phase value when the change exceeds $\pi$. Note that frequency hopping can also cause big variations between two back-to-back phase samples, and unwrapping will only be used for consecutive phase samples collected from the same channel. After the unwrapping operation, the phase samples from each channel is smoothed.

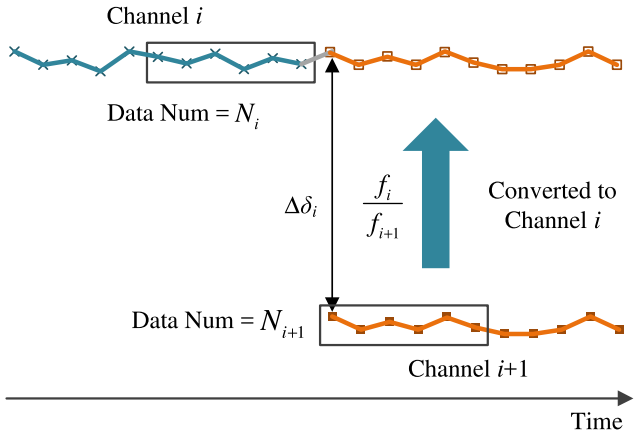


**FIGURE 5.** Illustration of the proposed frequency hopping offset mitigation scheme.

The second step is to splice the smoothed phase signals from all the 50 channels into a single phase signal, by mitigating the frequency hopping offsets. The key is to translate the phase signal from the next channel that the reader hops to, to a transformed phase signal using the previous channel as a reference with real-time calibration. As illustrated in Fig. 5, the phase signal from the previous channel, e.g., channel $i$, can be written as

$$\phi(f_i, d) = \mathrm{mod}\left(\frac{2\pi f_i d}{c} + \delta_i, 2\pi\right). \quad (3)$$

Then the reader hops from channel $i$ to channel $(i+1)$. Similarly, for the next channel that the reader hops to, we have

$$\phi(f_{i+1}, d) = \text{mod}\left(\frac{2\pi f_{i+1} d}{c} + \delta_{i+1}, 2\pi\right). \quad (4)$$

For simplifying notation, ignore the modulo operation for now. We then multiply the channel $(i+1)$ phase signal by a factor of $(f_i/f_{i+1})$, to have

$$\begin{aligned}\hat{\phi}(f_{i+1}, d) &= \phi(f_{i+1}, d) \times \frac{f_i}{f_{i+1}} \\ &= \frac{2\pi f_i d}{c} + \delta_{i+1} \times \frac{f_i}{f_{i+1}} \\ &\doteq \frac{2\pi f_i d}{c} + \delta_i + \Delta\delta_i, \quad i = 1, 2, ..., 49. \end{aligned} \quad (5)$$

Therefore, we have

$$\hat{\phi}(f_{i+1}, d) = \phi(f_i, d) + \Delta\delta_i, \quad i = 1, 2, ..., 49, \quad (6)$$

where

$$\Delta\delta_i \doteq \delta_{i+1} \times \frac{f_i}{f_{i+1}} - \delta_i, \quad (7)$$

represents the transformed phase offset, as illustrated in Fig. 5, which can be easily estimated as follows.

Note that we already know the frequency for each channel. So we first multiply the phase $\phi(f_{i+1}, d)$ collected from channel $(i+1)$ with a ratio $f_i/f_{i+1}$. The next value we need to calibrate is $\Delta\delta_i$ as in (7). In AutoTag, only three tags are attached to the human body. The overall sampling frequency of the reader is 600 Hz, and the sampling rate for each tag is more than 100 Hz. It takes only less than 1 ms for the reader to hop from one channel to another. Due to the high sampling rate and the small channel hopping time, it is reasonable to assume that the antenna-to-tag distance and the surrounding environment remain the same during channel hopping. Under this assumption, the difference between the phase data before channel hopping and the transformed phase data after channel hoping, is all caused by $\Delta\delta_i$ along with thermal noise.

To mitigate the influence of thermal noise, we apply a Hampel filter to the signal read from each channel. We choose a sliding window of 20 samples and a threshold of 0.01 for the Hampel filter. Next, we compute the difference between (i) the average of the last 6 phase readings in the previous channel $i$ (denoted as $\phi(f_i, d, k)$), and (ii) the average of the first 6 transformed phase readings in the present channel $(i+1)$ (denoted as $\hat{\phi}(f_{i+1}, d, k)$), as an estimate for the transformed phase offset $\Delta\delta_i$. As shown in Fig. 5, and also from (6), we have

$$\hat{\Delta}\delta_i \approx \frac{1}{6}\left(\sum_{k=N_i-5}^{N_i} \phi(f_i, d, k) - \sum_{k=0}^{5} \hat{\phi}(f_{i+1}, d, k)\right), \quad (8)$$

where $N_i$ is the total number of phase readings collected from channel $i$.

After compensating for the frequency hopping offset, the phase samples on the present channel $(i+1)$ can be approximated as in (6). Fig. 6 plots the calibrated phase samples after removing the frequency hopping offset. It can be seen that after calibration, the collected phase data shows an visible periodic respiration signal, which is completely missing in the uncalibrated phase data in Fig. 4 (for the same period of 28 seconds).

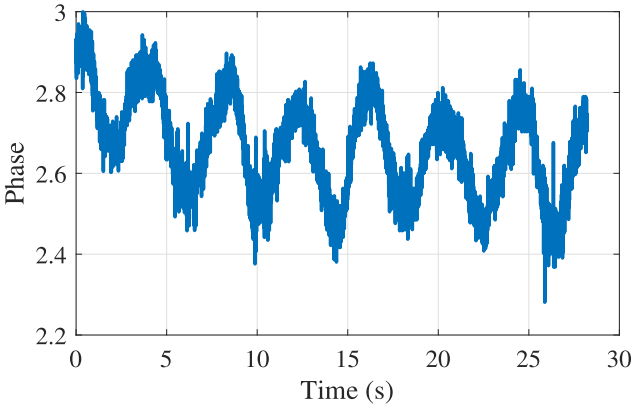


**FIGURE 6.** The resulting phase data after removing the frequency hopping offset.

### 2) MOVEMENT DETECTION

After mitigating the frequency hopping offset, the next step is to detect whether the patient is moving. Note that the breathing signal is very weak comparing to other types of body movement. Therefore, we should only use the signals collected while patient if in a stationary state, to avoid the interference introduced by large movements of human body.

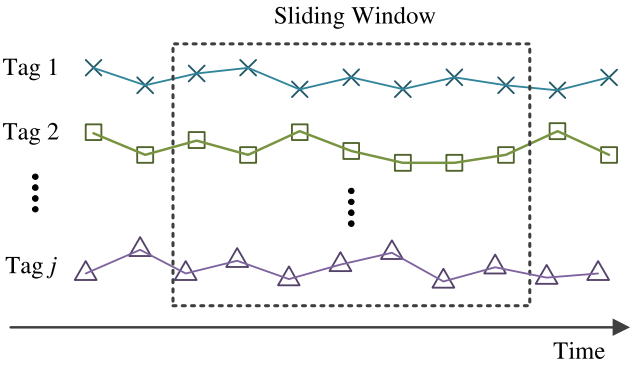


**FIGURE 7.** A sliding window on phase readings from the tags.

Movement detection is accomplished with a threshold based method. In particular, a sliding window is applied to the collected phase data, as showed in Fig. 7. For each window, we calculate the total mean absolute deviation of the phase samples from all tags, denoted by $T$, as

$$T = \frac{1}{|W|}\sum_{j=1}^{N}\sum_{k\in W} |\phi^j(k) - \mathbb{E}(\phi^j(k))|, \quad (9)$$

where $W$ represents the set of all the phase readings in the sliding window, $|\cdot|$ is the cardinality, $N$ is the number of tags, and $\phi^j(k)$ is the $k$th phase sample obtained from tag $j$.

If the patient is not stationary, the phase values will exhibit big changes (due to the large changes in $d$ caused by body movements). Thus, by setting a threshold on $T$, we can detect considerable movements of the patient. In AutoTag, we use a threshold value of 0.9 and a window size larger than 6 seconds for movement detection, based on our extensive experiments with various body movements.

#### 3) DC REMOVAL

Although the frequency hopping offset can be effective mitigated using a reference channel, the initial offset on the reference channel is still a random value that introduces a random DC component in the phase data. To remove the random DC component, as well as interference from other movements from the environment, we pass the phase signal through a detrending operation. Specifically, another Hampel filter is used, whose window size is 2000 and threshold is 0.001, to obtain an estimate of the DC component (i.e., the trend). Finally, the calibrated phase signal is obtained by subtracting the trend from the filtered signal. The calibrated signal is plotted in Fig. 8 for the same period of 28 s. It can be seen that the calibrated signal is now centered at zero, like a periodic AC signal.

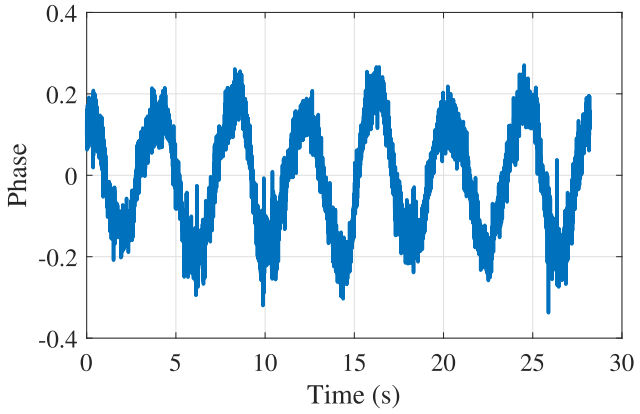


**FIGURE 8.** The calibrated phase signal after removing the DC component with a Hampel filter.

#### 4) TAG SELECTION

When analyzing the experimental results, we find that each tag has a different sensitivity to the human breathing signal from other tags, which depends on the slightly different tag parameters and the different propagation environment (e.g., distance or angle) of each tag. In particular, the angle between the tag and the reader antenna is a factor that causes the difference in tag's sensitivity. To obtain the most sensitive signal, we measure the signal strength using the average absolute deviation within a certain window size of 6 seconds (see (9)). The tag with the largest signal strength will be chosen for the remaining processing steps.

#### 5) DOWNSAMPLING AND FILTERING

Due to the high sampling frequency, i.e., about 600 Hz with one reader antenna, the signal need to be downsampled to reduce the computational complexity. In AutoTag, the signal is downsampled with a factor of 10 before feeding to the respiration monitoring module. In addition, there are still some false peaks introduced by thermal noises, which affect the accuracy of peak detection for respiration rate estimation. Note that the normal human respiration rate is usually much lower than 0.5 Hz. Thus, we apply a low-pass filter and choose a cutoff frequency of 0.5 Hz to the downsampled signal, in order to remove the remaining high frequency noise. In Fig. 9, we plot the downsample and filtered phase signal, which is quite smooth now. It is then used as input to the next module for the following apnea detection and respiration rate estimation tasks.

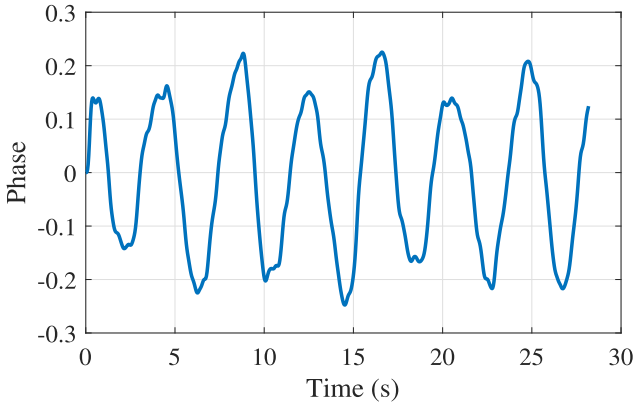


**FIGURE 9.** The finally recovered respiration signal.

### D. APNEA DETECTION AND RESPIRATION RATE ESTIMATION

#### 1) RECURRENT VARIATIONAL AUTOENCODER FOR APNEA DETECTION

For the purpose of accurate respiration detection, we introduce a recognition model as an approximation to the intractable true posterior, where the parameters are not computed from some closed-form expectation, but are learned from the calibrated data. To detect apnea, the main idea of AutoTag is to incorporate a *variational autoencoder* to compute the difference between the sampled signal and the reconstructed signal within a time window. Note that this is an unsupervised learning [32], [33], with the desirable advantage of not requiring labeled medical data that is hard or costly to obtain. If the computed difference is smaller than a given threshold, the sampled signal is regarded as a regular breathing signal, from which the respiration rate can be estimated; otherwise, the signal sequence is regarded to be abnormal, and apnea is detected. Since the energy based threshold has been applied for movement detection in the earlier stage (see Section IV-C2), small breathing signals can be detected now at this stage.

The proposed recurrent variational autoencoder for unsupervised respiration abnormality detection is illustrated in Fig. 10. We first apply the variational autoencoder model to obtain a reconstructed version of the input signal. This model

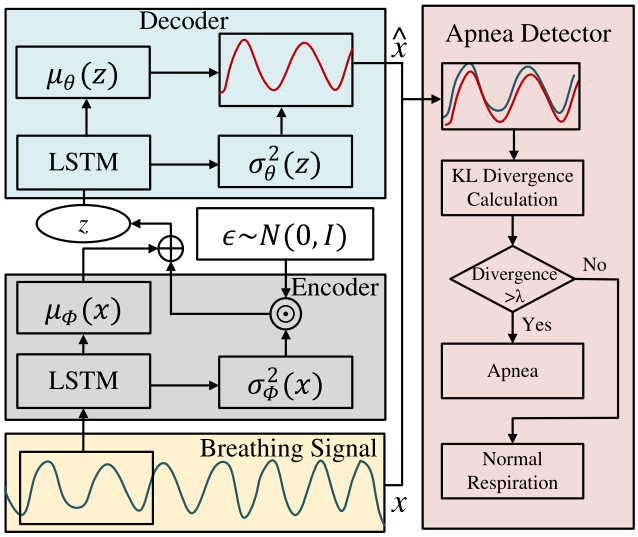


**FIGURE 10.** Architecture of the proposed recurrent variational autoencoder for unsupervised apnea detection.

is to maximize the marginal likelihood given below.

$$p_\theta(x) = \int p_\theta(x|z)p(z)dz, \tag{10}$$

where $x$, $z$, and $\theta$ are the observed variables, the latent random variables, and the set of parameters, respectively; $p(z)$ is the prior over the latent random variables $z$; and $p_\theta(x|z)$ is the conditional probability, representing an observation model under the parameter set. Usually $p_\theta(x)$ is intractable due to the integral operation. Although the Monte Carlo sampling method can be used to solve the problem, it usually incurs a considerable computational cost even for small-sized datasets. The variational autoencoder model utilizes the variational approximation $q_\phi(z|x)$ instead of the true posterior $p_\theta(z|x)$. Specifically, the variational autoencoder model has $q_\phi(z|x)$ with parameter set $\phi$ as encoder and $p_\theta(x|z)$ with parameter set $\theta$ as decoder. According to Jensen's inequality, the variational autoencoder model can achieve the optimal values for sets $\phi$ and $\theta$. This is achieved by maximizing a lower bound on the log-likelihood, given by [32]

$$\max \mathcal{L} = -D_{KL}(q_\phi(z|x)||p(z)) + \mathbb{E}_{z\in q_\phi(z|x)}\left[p_\theta(x|z)\right], \tag{11}$$

where $D_{KL}$ represents the KL divergence. In (11), $-D_{KL}(q_\phi(z|x)||p(z))$ represents the regularization over the latent variables $z$, while $\mathbb{E}_{z\in q_\phi(z|x)}\left[p_\theta(x|z)\right]$ is the autoencoder. The latent variables $z$ are sampled from $q_\phi(z|x)$, and the reconstructed signal $\hat{x}$ can be sampled from $p_\theta(x|z)$.

To reduce the training overhead, the variational autoencoder model utilizes the reparametrization technique. With this technique, the latent vector $z$ is computed from the mean vector $\mu_\phi(x)$ and the variance vector $\sigma^2_\phi(x)$, as

$$z = \mu_\phi(x) + \sigma_\phi(x) \odot \epsilon, \tag{12}$$

where $\epsilon \in \mathcal{N}(0, 1)$ (i.e., a standard Gaussian distribution), and $\odot$ represents the element-wise product operation. The lower bound on the log-likelihood, i.e., $\mathcal{L}$, can then be approximated as follows.

$$\mathcal{L} \approx \frac{1}{2}\sum_{j=1}^{J}\left(1 + \log(\sigma_j^2(x)) - \mu_j^2(x) - \sigma_j^2(x)\right) + \frac{1}{M}\sum_{l=1}^{M}\log p_\theta(x|z_l), \tag{13}$$

where $M$ is the number of samples in $z$, and $J$ is the cardinality of $z$.

Next, we consider the data samples within a time window, to be processed by a long short-term memory (LSTM) network. LSTM belongs to the class of recurrent neural networks (RNN) that can effectively handle time series data. It can also deal with the problem of vanishing gradient in RNNs. The long-range dependencies in the data can be effectively captured by LSTM, because the data in a time series can be stored or deleted by a non-linear gate in each unit. In the proposed AutoTag system, LSTM is utilized to encode the respiration signal sequence within a time window. Then its outputs are used to obtain estimations for the mean vector $\mu_\phi(x)$ and the variance vector $\sigma^2_\phi(x)$ using two linear modules, respectively. The sampled $z$ is fed to another LSTM network for decoding the estimated mean and variance vectors. Eventually we obtain a reconstructed respiration signal for the same time window.

Once the reconstructed respiration signal is obtained, we propose a KL divergence based method for apnea detection. Specifically, we first normalize both the original signal and the reconstructed signal in the same time window, in order to ensure that both the apnea signal and the respiration signal are within the same amplitude range. The similarity between the original signal and the reconstructed signal is then calculated in the form of KL divergence. Since the proposed neural network is well trained by a large amount of normal breathing signal, the KL divergence between the input signal and the reconstructed signal is very small when the signal is sampled during normal breathing. In contrast, the KL divergence will be very large when the input signal includes abnormal respiration (apnea), because the network does not know the features of the abnormalities. Finally, we collect the values of KL divergence calculated for normal breathing and apnea, respectively, and a threshold $\lambda$ is properly chosen to determine whether the signal in this time window is from apnea or normal respiration. Specifically, if the KL divergence is greater than the threshold, apnea is detected in this time window; otherwise, the signal is from normal respiration.

The proposed deep learning based approach has two desirable features. First, the recurrent variational autoencoder is an unsupervised learning. Therefore, there is no need to collect labeled data for regular and abnormal respiration signals, which could be costly and time consuming. Second, the proposed method can learn the periodic features of respiration signal in offline training, rather than simply detecting the

strength of the breathing signal. Therefore, this method is superior to the energy threshold based method, especially when the patient moves.

#### 2) PEAK DETECTION FOR BREATHING RATE ESTIMATION

Finally, the peak detection technique [11] is used to estimate the interval between two neighboring peaks, when a regular respiration signal is detected. Although most of the noise coming from the environment have been removed at this stage, some false peaks may still exist. False peaks are usually relatively smaller than the peaks of the respiration signal, but they still could affect the accuracy of peaks detection.

To mitigate the influence of such false peaks, we execute the peak detection algorithm with a small sliding window of data points, instead of on the entire sampled signal sequence. In AutoTag, a window size of 11 data points are used. Only if the center data point of the sliding window is the maximum among all the data points within the window, the center data point will be identified as a peak. Then the mean value of all the peak intervals is calculated to approximate the period of the respiration signal $\tau$. Finally, the respiration rate can be computed as $60/\tau$ breaths per minute (bpm).

## V. PROTOTYPING, EXPERIMENTS, AND DISCUSSIONS

### A. PROTOTYPING AND EXPERIMENTAL ENVIRONMENTS

To evaluate the proposed AutoTag system, we adopt Impinj R420 as the RFID reader to collect phase information from ALN-9740 tags. To be FCC-compliant, the circular polarized antenna equipped in our system hops among 50 channels ranging from 902.5 MHz to 927.5 MHz, and remains on each channel for 200 ms. The user interface and the signal processing is implemented with an MSI laptop equipped with a Nvidia GTX1080 GPU and an Intel(R) Core(TM) i7-6820HK CPU. A software is also implemented in our system to collect data from the reader using the Low-level Reader Protocol (LLRP), which can extract useful low-level data from received tag responses, including time stamp, Doppler shift, RSSI, and phase value.

We carry out extensive experiments that involve four volunteers. The experimental results in two different environments are presented in this section. The test settings include a 5.6 m $\times$ 7.5 m lab, which is cluttered with tables, chairs, and computers, and a 2.4 m $\times$ 20.0 m empty corridor with no moving persons in Broun Hall in the Auburn University Campus. In the lab setting, the multipath effect is obviously larger than that in the corridor setting. All the volunteers are tested in three cases: (i) sitting in a chair and breathing normally, (ii) sitting in the chair and holding breath, and (iii) moving randomly while breathing normally.

For respiration rate estimation, we obtain the cumulative distribution function (CDF) of estimation errors for performance validation. For apnea detection, the following two performance metrics are used:

- True Negative (TN) rate: this is the success rate when a regular respiration signal is successfully detected;
- True Positive (TP) rate: this is the success rate when apnea is correctly detected.

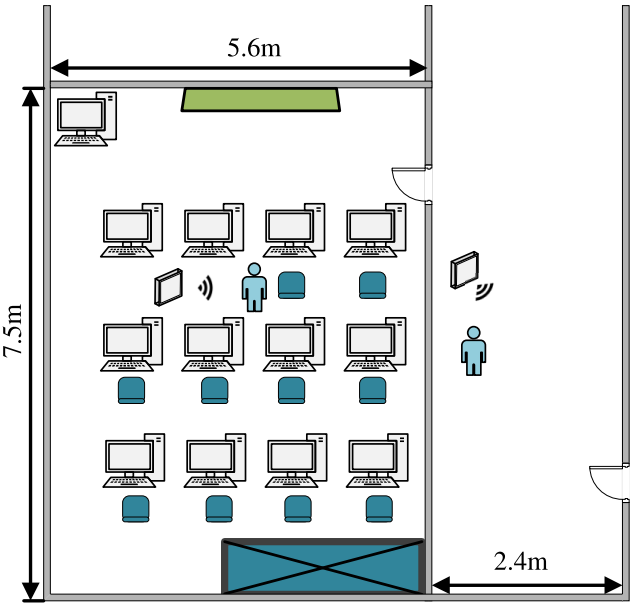


**FIGURE 11.** Experimental environments for validating the performance of AutoTag. (i) A cluttered computer laboratory. (ii) An empty corridor.

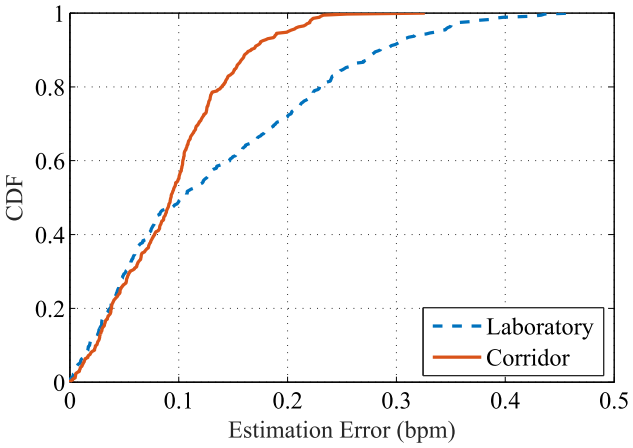


**FIGURE 12.** CDFs of estimated breathing rates in the computer lab and corridor scenarios.

### B. EXPERIMENTAL RESULTS AND DISCUSSIONS

For the normal breathing scenario, we evaluate the accuracy of respiration rate estimation under the two settings. We also use the NEULOG Respiration Belt sensor wrapped on the volunteer's chest to measure the ground truth. The CDFs of estimation errors are plotted in Fig. 12 for the lab and corridor experiments. We find the maximum errors are 0.462 bpm and 0.326 bpm, while the median errors are 0.105 bpm and 0.093 bpm, for the lab and corridor settings, respectively. The maximum and median errors in the lab setting are both larger than the corresponding error in the corridor setting.

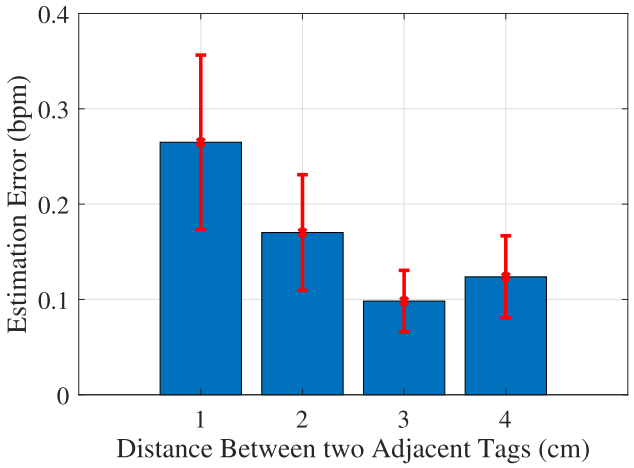


**FIGURE 13.** Evaluating the effect of the distance between two neighboring RFID tags.

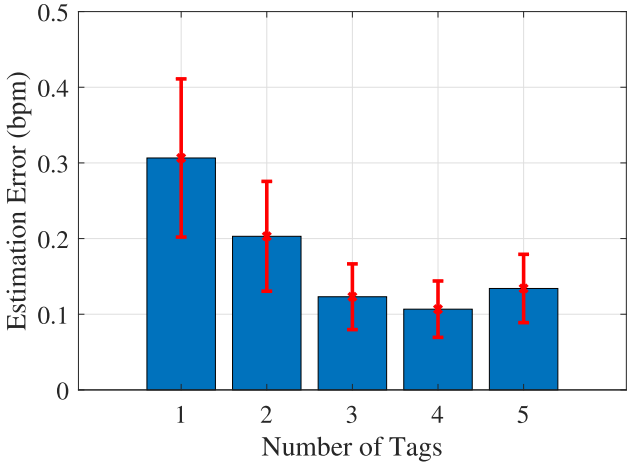


**FIGURE 14.** Evaluating the effect of the number of attached RFID tags.

In addition, more than 50% estimation errors obtained in the corridor setting are smaller than that obtained in the lab setting. These indicate that the multipath effect does affect the accuracy of respiration rate estimation. Furthermore, it can be seen that the median error in the lab and corridor tests are 0.104 bpm and 0.0925 bpm, respectively. The close median errors indicate that the effect of multipath is not substantial. Since a directional antenna is used by the reader, the backscattered tag response in the line-of-sight (LOS) path is the dominant component. Thus, the respiration rate estimation in the two settings are both accurate.

We also study the influence of various factors on the estimation precision of our system. Fig. 13 plots the impact of the distance between two adjacent tags. We test the system with a tag array attached to the human chest with different distances between adjacent tags. The figure shows that when the distance between two tags is 1 cm, the estimation error is 0.265 bpm, which is relatively large. This is because when tags are too close to each other, they will suffer from stronger mutual coupling effect. The measured phase will be distorted by mutual coupling, and thus the estimated respiration rate will also be affected. Fortunately, the figure also reveal that when the tags are more than 2 cm apart, the error will become smaller than 0.124 bpm, which indicates the influence of mutual coupling is negligible in these cases. Therefore, we deployed the tags with a 3 cm tag-interval in the AutoTag system.

Fig. 14 presents the influence of the number of tags used in AutoTag. We test the system with an increased number of tags from 1 to 5, while the tag distance is set to 3 cm. As can be seen in the figure, the estimation error is higher than 0.307 bpm when only one tag is used.When 3 or more tags are used, the error becomes smaller than 0.134 bpm. This is because the sensitivity of the single tag is more susceptible to the propagation environment, such as different surroundings and human postures. When multiple tags are used, we select the most sensitive tag to measure the human respiration, which increases the sensitivity of the system. Based on the results showed in Fig. 14, we adopt 3 tags on the volunteers to increase the accuracy of our system.

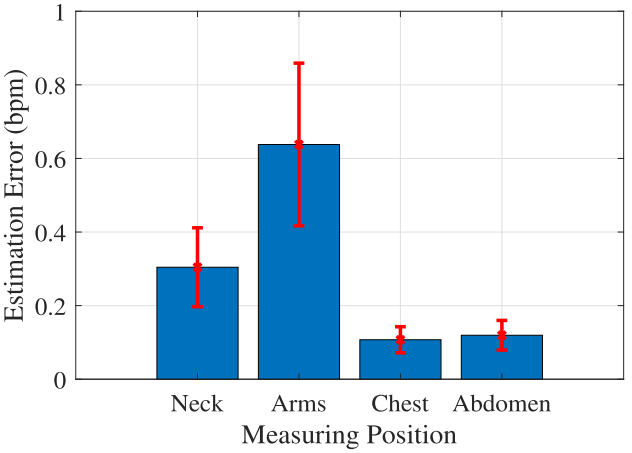


**FIGURE 15.** Evaluating the effect of different measuring positions.

We also experiment by placing tags on different parts of the human body. Fig. 15 shows that, the estimation error is large when the tags are placed on the arms and neck of the volunteers, which are 0.637 bpm and 0.304 bpm, respectively. When the tags are placed on the chest and abdomen, the error becomes lower than 0.119 bpm. This is because respiration directly causes the chest and abdomen to move. When the tags are placed on the neck and arms, the strength of the movement, and thus the phase signal is not strong enough for effectively extraction of respiration signal, although the backscattered signal is also reflected from the chest. In addition, the arm movements generate a large noise, which also affect the accuracy of the system. Therefore, all the tags are attached to the human chest or abdomen in the AutoTag system.

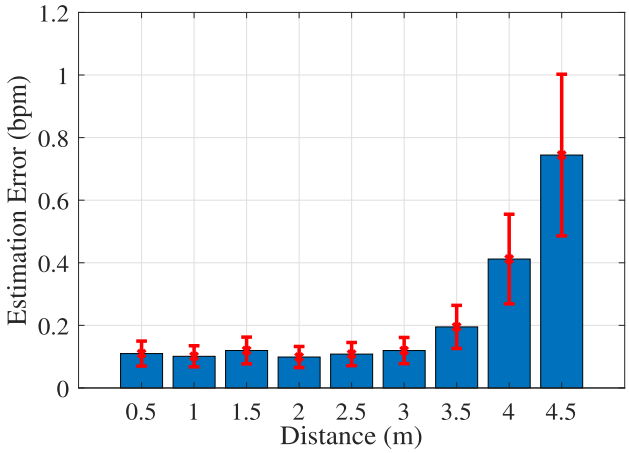


**FIGURE 16.** Evaluating the effect of the distance between the patient chest and reader antenna.

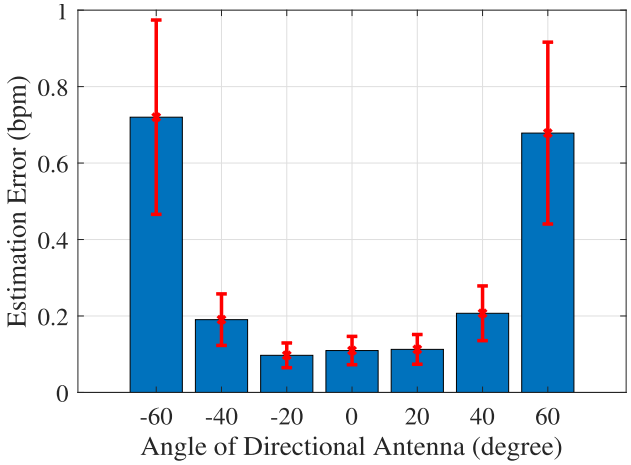


**FIGURE 17.** Evaluating the effect of the angle of the directional reader antenna.

Next, the effective rage of our system is evaluated, and the results are presented in Fig. 16 and Fig. 17. Fig. 16 presents the estimation errors at different distances between the patient and the antenna. We find that the respiration rate error is less than 0.112 bpm when the distance is shorter than 3.5 m. The error increases drastically when the distance becomes larger than 4 m. To evaluate the impact of the angle of the directional antenna, we measure the respiration rate at a fixed distance with various relative orientation angles between the patient and the directional antenna: where 0° means the antenna directly faces the patient. As show in Fig. 17, the estimation error is smaller than 0.127 bpm when the angle is between $-20°$ and 20°. The error increases to be larger than 0.678 bpm when the angle is beyond $\pm 60°$. This is because the received power of the backscattered signal is different at different radiation angles for the directional antenna. According to the results presented in Figs. 16 and 17, we conclude that the distance between the patient and the antenna should be less than 3 m and the orientation angle of the antenna should be within $\pm 20°$.

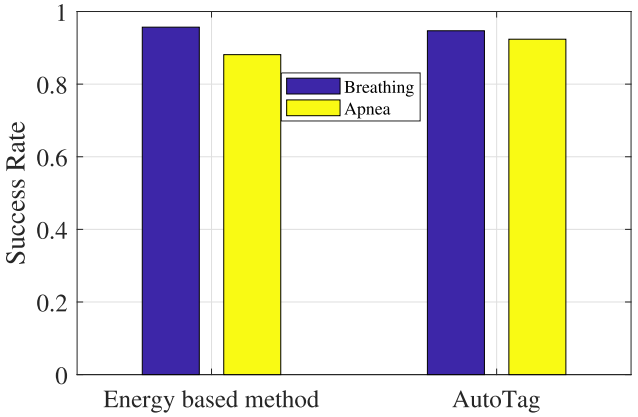


**FIGURE 18.** True Negative rate and true Positive rate obtained in a stable setting.

We also study the proposed AutoTag system by comparing with an energy based baseline method [34] under two different settings. In the first setting, the patient sits quietly with no other movements than breathing; in the second setting, the patient is allowed to move slightly, such as moving legs and hands, and twisting neck. Fig. 18 provides the TN and TP rates obtained with the proposed method and the baseline method in the stationary setting. When there are no body movements, the TN rates are both over 94% for the proposed and baseline schemes. Furthermore, the TP rates are 88% and 92% for the proposed and baseline schemes, respectively. These results indicate that both AutoTag and the energy based baseline method can achieve considerably high TN and TP rates when the patient does not make slight moves.

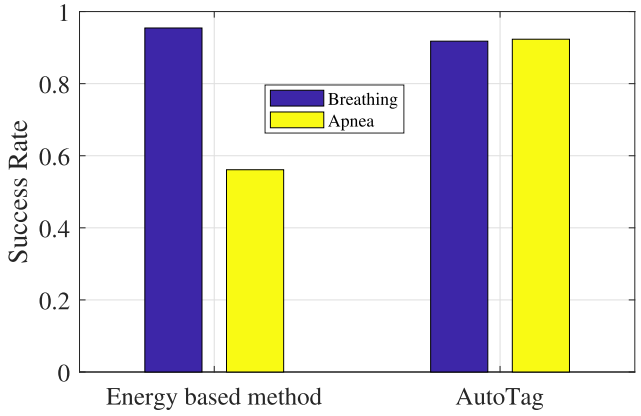


**FIGURE 19.** True negative rate and true positive rate obtained when there are small body movements.

When the patient moves slightly, however, the situation becomes quite different. The results under slight body movements are given in Fig. 19. We find the TP rate of the energy based baseline scheme drops to 56%, but the TP rate of AutoTag is still as high as 92%. Under the disturbance of small body movements, the energy of the apnea signal can be greatly increased. It is therefore challenging to choose

a suitable threshold for apnea detection in the baseline scheme. In contrast, AutoTag detects respiration abnormality by matching the shapes of the original and reconstructed signals; it does not rely on the signal's energy level. Consequently, AutoTag is resilient to the energy disturbance caused by small body movements in this setting. Furthermore, as shown in Fig. 19, the TN rates achieved by AutoTag and the baseline scheme are both above 91%, which are only slightly less than the TN rates achieved in the stationary setting (although the body movements also distort the shape of the respiration signal). We conclude that AutoTag system can accurately detect apnea and normal respiration signals in the two settings.

## VI. CONCLUSIONS

This paper presented the AutoTag system for unsupervised respiration rate estimation and detection of apnea in real-time with commodity RFID Tags. The AutoTag system incorporated a novel technique to effectively address the effect of frequency hopping offset for RFID systems that comply to FCC regulations, and thus can be used for many RFID applications with real-time requirements. The proposed system also incorporated an unsupervised learning, thus has the desirable advantage of not requiring labeled medical data, making it low-cost and easy to deploy. The superior performance of the AutoTag system is demonstrated by extensive experiments in typical healthcare environments.

## ACKNOWLEDGMENT

This work was presented in part at the IEEE GLOBECOM 2018, Abu Dhabi, UAE, December 2018 [1].

## REFERENCES

[1] C. Yang, X. Wang, and S. Mao, "AutoTag: Recurrent variational autoencoder for unsupervised apnea detection with RFID tags," in *Proc. IEEE GLOBECOM*, Abu Dhabi, UAE, Dec. 2018, pp. 1–7.

[2] O. Boric-Lubeke and V. M. Lubecke, "Wireless house calls: Using communications technology for health care and monitoring," *IEEE Microw. Mag.*, vol. 3, no. 3, pp. 43–48, Sep. 2002.

[3] X. Wang, X. Wang, and S. Mao, "RF sensing in the Internet of Things: A general deep learning framework," *IEEE Commun.*, vol. 56, no. 9, pp. 62–67, Sep. 2018.

[4] X. Wang, R. Huang, and S. Mao, "SonarBeat: Sonar phase for breathing beat monitoring with smartphones," in *Proc. ICCCN*, Vancouver, BC, Canada, Jul./Aug. 2017, pp. 1–8.

[5] C. E. Hunt and F. R. Hauck, "Sudden infant death syndrome," *Can. Med. Assoc. J.*, vol. 174, no. 13, pp. 1861–1869, Jun. 2006.

[6] L. R. Mogue and B. Rantala, "Capnometers," *J. Clin. Monit.*, vol. 4, no. 2, pp. 115–121, Apr. 1988.

[7] F. Adib, H. Mao, Z. Kabelac, D. Katabi, and R. C. Miller, "Smart homes that monitor breathing and heart rate," in *Proc. ACM CHI*, Seoul, South Korea, Apr. 2015, pp. 837–846.

[8] P. Nguyen, X. Zhang, A. Halbower, and T. Vu, "Continuous and fine-grained breathing volume monitoring from afar using wireless signals," in *Proc. IEEE INFOCOM*, San Francisco, CA, USA, Apr. 2016, pp. 1–9.

[9] H. Abdelnasser, K. A. Harras, and M. Youssef, "Ubibreathe: A ubiquitous non-invasive WiFi-based breathing estimator," in *Proc. IEEE MobiHoc*, Hangzhou, China, Jun. 2015, pp. 277–286.

[10] J. Liu, Y. Wang, Y. Chen, J. Yang, X. Chen, and J. Cheng, "Tracking vital signs during sleep leveraging off-the-shelf WiFi," in *Proc. ACM Mobihoc*, Hangzhou, China, Jun. 2015, pp. 267–276.

[11] X. Wang, C. Yang, and S. Mao, "PhaseBeat: Exploiting CSI phase data for vital sign monitoring with commodity WiFi devices," in *Proc. IEEE ICDCS*, Atlanta, GA, USA, Jun. 2017, pp. 1–10.

[12] X. Wang, C. Yang, and S. Mao, "TensorBeat: Tensor decomposition for monitoring multiperson breathing beats with commodity WiFi," *ACM Trans. Intell. Syst. Technol.*, vol. 9, no. 1, Oct. 2017, Art. no. 8.

[13] X. Wang, C. Yang, and S. Mao, "ResBeat: Resilient breathing beats monitoring with realtime bimodal CSI data," in *Proc. IEEE GLOBECOM*, Singapore, Dec. 2017, pp. 1–6.

[14] L. Yang, Y. Chen, X.-Y. Li, C. Xiao, M. Li, and Y. Liu, "Tagoram: Real-time tracking of mobile RFID tags to high precision using COTS devices," in *Proc. ACM MobiCom*, Maui, HI, USA, Sep. 2014, pp. 237–248.

[15] T. Wei and X. Zhang, "Gyro in the air: Tracking 3D orientation of batteryless Internet of Things," *ACM GetMobile*, vol. 21, no. 1, pp. 35–38, Mar. 2017.

[16] Y. Ma, N. Selby, and F. Adib, "Drone relays for battery-free networks," in *Proc. ACM SIGCOMM*, Los Angeles, CA, USA, Aug. 2017, pp. 335–347.

[17] J. Zhang, Z. Yu, X. Wang, Y. Lyu, S. Mao, S. C. Periaswamy, J. Patton, and X. Wang "RFHUI: An intuitive and easy-to-operate human-UAV interaction system for controlling a UAV in a 3D space," in *Proc. EAI MobiQuitous*, New York, NY, USA, Nov. 2018, pp. 69–76.

[18] J. Zhang, Z. Yu, X. Wang, Y. Lyu, S. Mao, S. C. G. Periaswamy, J. Patton, and X. Wang, "RFHUI: An RFID based human-unmanned aerial vehicle interaction system in an indoor environment," *Digit. Commun. Netw.*, to be published. doi: 10.1016/j.dcan.2019.05.001.

[19] Y. Hou, Y. Wang, and Y. Zheng, "TagBreathe: Monitor breathing with commodity RFID systems," in *Proc. IEEE ICDCS*, Atlanta, GA, USA, Jun. 2017, pp. 404–413.

[20] J. Chung, K. Kastner, L. Dinh, K. Goel, A. C. Courville, and Y. Bengio, "A recurrent latent variable model for sequential data," in *Proc. NIPS*, Montreal, QC, Canada, Dec. 2015, pp. 2980–2988.

[21] I. Habibie, D. Holden, J. Schwarz, J. Yearsley, and T. Komura, "A recurrent variational autoencoder for human motion synthesis," in *Proc. Brit. Mach. Vis. Conf.*, London, U.K., Sep. 2017, pp. 1–12.

[22] J. Salmi and A. F. Molisch, "Propagation parameter estimation, modeling and measurements for ultrawideband MIMO radar," *IEEE Trans. Antennas Propag.*, vol. 59, no. 11, pp. 4257–4267, Nov. 2011.

[23] L. M. Ni, Y. Liu, Y. C. Lau, and A. P. Patil, "LANDMARC: Indoor location sensing using active RFID," in *Proc. 1st IEEE PerCom*, Dallas, TX, USA, Mar. 2003, pp. 407–415.

[24] H. Ding, J. Han, C. Qian, F. Xiao, G. Wang, N. Yang, W. Xi, and J. Xiao, "Trio: Utilizing tag interference for refined localization of passive RFID," in *Proc. IEEE INFOCOM*, Honolulu, HI, USA, Apr. 2018, pp. 828–836.

[25] J. Wang, D. Vasisht, and D. Katabi, "RF-IDraw: Virtual touch screen in the air using RF signals," *ACM SIGCOMM Comput. Commun. Rev.*, vol. 44, no. 4, pp. 235–246, Oct. 2014.

[26] W. Jue and D. Katabi, "Dude, where's my card? RFID positioning that works with multipath and non-line of sight," *ACM SIGCOMM Comput. Commun. Rev.*, vol. 43, no. 4, pp. 51–62, Aug. 2013.

[27] L. Shangguan and K. Jamieson, "The design and implementation of a mobile RFID tag sorting robot," in *Proc. ACM MobiSys*, Singapore, Jun. 2016, pp. 31–42.

[28] T. Liu, L. Yang, Q. Lin, Y. Guo, and Y. Liu, "Anchor-free backscatter positioning for RFID tags with high accuracy," in *Proc. IEEE INFOCOM*, Toronto, ON, Canada, Apr./May 2014, pp. 379–387.

[29] X. Wang, J. Zhang, Z. Yu, E. Mao, S. Periaswamy, and J. Patton, "RF Thermometer: A temperature estimation method with commercial UHF RFID tags," in *Proc. IEEE ICC*, Shanghai, China, May 2019, pp. 1–6.

[30] C. Wang, J. Liu, Y. Chen, H. Liu, L. Xie, W. Wang, B. He, and S. Lu, "Multi—Touch in the air: Device-free finger tracking and gesture recognition via COTS RFID," in *Proc. IEEE INFOCOM*, Honolulu, HI, USA, Apr. 2018, pp. 1691–1699.

[31] Impinj Support Portal, Impinj Speedway Revolution Reader Application. (2013). *Low Level User Data Support*. [Online]. Available: https://support.impinj.com

[32] D. P. Kingma and M. Welling, "Auto-encoding variational bayes," May 2014, *arXiv:1312.6114*. [Online]. Available: https://arxiv.org/abs/1312.6114

[33] O. Fabius and J. R. van Amersfoort, "Variational recurrent auto-encoders," Jun. 2015, *arXiv:1412.6581*. [Online]. Available: https://arxiv.org/abs/1412.6581

[34] L. Almazaydeh, K. Elleithy, M. Faezipour, and A. Abushakra, "Apnea detection based on respiratory signal classification," *Procedia Comput. Sci.*, vol. 21, pp. 310–316, 2013.

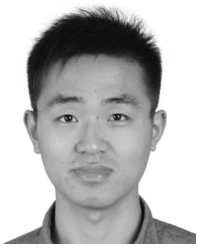

**CHAO YANG** received the B.E. degree in electrical engineering from Yanshan University, Hebei, China, in 2015, and the M.S. degree in electrical and computer engineering from Auburn University, Auburn, AL, USA, in 2017, where he is currently pursuing the Ph.D. degree in electrical and computer engineering. His current research interests include health sensing, indoor localization, the Internet of Things, and wireless networks.

**XUYU WANG** received the B.S. in degree in electronic information engineering and the M.S. degree in signal and information processing from Xidian University, Xi'an, China, in 2009 and 2012, respectively, and the Ph.D. degree in electrical and computer engineering from Auburn University, Auburn, AL, USA, in 2018. He is currently an Assistant Professor with the Department of Computer Science, California State University, Sacramento, CA, USA. His research interests include deep learning, the Internet of Things, indoor localization, RFID sensing, computer vision, health sensing, and wireless systems. He was a co-recipient of the Second Prize of the Natural Scientific Award of Ministry of Education, China, in 2013, the Best Demo Award from the IEEE SECON 2017, the Best Student Paper Award from the IEEE PIMRC 2017, and the IEEE ComSoc MMTC Best Journal Paper Award, in 2019.

**SHIWEN MAO** (S'99–M'04–SM'09–F'19) received the Ph.D. degree in electrical and computer engineering from Polytechnic University, Brooklyn, NY, USA, (now The New York University Tandon School of Engineering).

He was the McWane Associate Professor, from 2012 to 2015. He is currently a Samuel Ginn Distinguished Professor with the Department of Electrical and Computer Engineering and the Director of the Wireless Engineering Research and Education Center, Auburn University, Auburn, AL, USA. His research interests include wireless networks, multimedia communications, and smart grids. He has been a Distinguished Speaker, since 2018, and was a Distinguished Lecturer of the IEEE Vehicular Technology Society, from 2014 to 2018.

Dr. Mao has received the NSF CAREER Award in 2010, the 2013 IEEE ComSoc MMTC Outstanding Leadership Award, the 2015 IEEE ComSoc TC-CSR Distinguished Service Award, the 2017 IEEE ComSoc ITC Outstanding Service Award, the Auburn University Creative Research and Scholarship Award in 2018, the IEEE ComSoc TC-CSR Distinguished Technical Achievement Award in 2019, and the IEEE ComSoc MMTC Distinguished Service Award in 2019. He was a co-recipient of the IEEE ComSoc MMTC Best Journal Paper Award, in 2019, the IEEE ComSoc MMTC Best Conference Paper Award, in 2018, the Best Demo Award from the IEEE SECON 2017, the 2004 IEEE Communications Society Leonard G. Abraham Prize in the Field of Communications Systems, and the Best Paper Award from the IEEE ICC 2013, the IEEE WCNC 2015, and the IEEE GLOBECOM 2015 and 2016. He is on the Editorial Board of the IEEE TRANSACTIONS ON NETWORK SCIENCE AND ENGINEERING, the IEEE TRANSACTIONS ON MOBILE COMPUTING, the IEEE TRANSACTIONS ON MULTIMEDIA, the IEEE INTERNET OF THINGS JOURNAL, the IEEE MULTIMEDIA, the IEEE NETWORKING LETTERS, and ACM *GetMobile*.